Materials Today Communications 41 (2024) 110876

Contents lists available at ScienceDirect

Materials Today Communications

journal homepage: www.elsevier.com/locate/mtcomm

Electrocatalytic trends of different Cantor entropy alloys for alkaline and acidic hydrogen-evolution reactions

Barbara Ljubec Božiček [a,b,*], Bor Arah [c], Monika Kušter [a,b], Iztok Naglič [d], Boštjan Markoli [d], Maja Ponikvar-Svet [e], Lara Einfalt [a,b], Miran Čeh [a,c], Belisa Alcantara Marinho [a,**]

[a] Department for Nanostructured Materials, Jožef Stefan Institute, Jamova 39, Ljubljana 1000, Slovenia
[b] Jožef Stefan International Postgraduate School, Jamova 39, Ljubljana 1000, Slovenia
[c] Center for Electron Microscopy and Microanalysis, Jožef Stefan Institute, Jamova 39, Ljubljana 1000, Slovenia
[d] Department of Materials and Metallurgy, Faculty of Natural Sciences and Engineering, University of Ljubljana, Aškerčeva cesta 12, Ljubljana 1000, Slovenia
[e] Department of Inorganic Chemistry and Technology, Jožef Stefan Institute, Jamova 39, Ljubljana 1000, Slovenia

ARTICLE INFO

Keywords:
Medium-entropy alloy
High-entropy alloy
Water splitting
Hydrogen binding energy
Spillover effect

ABSTRACT

Medium- and high-entropy alloys (MEAs and HEAs) are the basis of unique electrocatalysts for hydrogen-evolution reactions (HERs) due to their tunable chemical compositions and microstructures. Here, various Cantor MEAs (CoFeNi, CoFeNiMn, CoFeNiCr) and a HEA (CoFeNiMnCr) made up of affordable non-noble transitional metals with different structures (primary matrix and secondary phases, grain sizes, lattice parameters) were successfully synthesized with an inert-gas melting process. A close correlation was established between their physicochemical properties (elemental composition, microstructure, crystal structure) and the hydrogen-binding ability of the elements in the alloy on the electrocatalytic HER activity and stability in alkaline and acidic media. Advanced performances of electrocatalysts toward HERs were revealed in a specially designed electrochemical cell. Effectively identifying these electrocatalytic trends lays the groundwork for the strategic design of multi-component alloy electrocatalysts for practical HERs.

1. Introduction

Hydrogen energy is one of the pathways to a sustainable, low-carbon future [1]. At present, the majority of hydrogen gas (over 95 %) is produced from fossil fuels. However, this process causes serious environmental problems. The electrochemical water-splitting utilizing renewable energy sources (e.g. solar, wind) represents a promising method for producing high purity and environmentally friendly green hydrogen [2]. The process consists of two half-reactions, the cathodic hydrogen evolution reaction (HER) and the anionic oxygen evolution reaction (OER) [3]. The intense focus lies especially in the HER process in order to support the sustainable hydrogen economy. Until now, platinum (Pt) and Pt-based noble metals have been considered to be the best electrocatalysts for HER, but high costs and limited abundance limit their broader application [4]. Therefore, a lot of effort has been dedicated to developing an alternative, non-noble electrocatalyst with high catalytic activity and stability in alkaline and acidic conditions.

Recently, the so-called entropy alloys have attracted a lot of interest as new catalytic-material platforms due to their unique physical and chemical properties originating from their compositional and structural complexity. As such, they form entropy-stabilized solid solutions with sluggish diffusion and cocktailing effects. These materials also have a highly disordered structure and randomly distributed components, advantageous for inducing fewer defects/vacant sites and strengthening the interaction between different atoms, which provides more active sites and promotes their activity, respectively [5,6]. All these features affect the electronic structure of the material, which is reflected in its catalytic properties, including the position of the d-band and the ability to bind hydrogen [7].

In this aspect, the Cantor medium- (MEA) and high-entropy alloys (HEA) show promising catalytic activity and stability toward electrochemical HER. For example, CoFeNi nanoparticles on carbon nanofibers exhibited an overpotential of 410 mV at 100 mA/cm^2 and a Tafel slope of 180.9 mV/dec in 1 M KOH [8]. F. McKay et al. [9] studied the potential application of arc melted, near equimolar CoCrFeNi for acidic HER, where the electrocatalyst showed an overpotential of 60 mV at

* Corresponding author at: Department for Nanostructured Materials, Jožef Stefan Institute, Jamova 39, Ljubljana 1000, Slovenia.
** Corresponding author.
E-mail addresses: barbara.ljubec.bozicek@ijs.si (B. Ljubec Božiček), belisa.alcantara.marinho@ijs.si (B. Alcantara Marinho).

https://doi.org/10.1016/j.mtcomm.2024.110876
Received 8 August 2024; Received in revised form 23 October 2024; Accepted 1 November 2024
Available online 4 November 2024

1 mA/cm^2 relative to Pt and only minor dissolution of elements without significant loss of activity after 1000 cycles. However, there is still insufficient information about the effect of the elemental composition and microstructure of the entropy alloys on the HER in different media.

In this study, three MEAs (CoFeNi, CoFeNiMn, and CoFeNiCr) and one HEA (CoFeNiMnCr), all with face-centered cubic (FCC) structures, were synthesized by melting in a tube furnace with an inert atmosphere. The synthesized materials were used as electrocatalysts for a HER in 1 M KOH and 0.5 M H_2SO_4 media. Correlations between the physicochemical and electrocatalytic properties affecting the HER are presented and discussed.

2. Materials and methods

The MEA and HEA ingots were prepared (Fig. S1) by melting the metal mixture at 1550 °C for 1 h and then annealing at 1000 °C for 24 h under an argon atmosphere. The CoFeNi and CoFeNiMn ingots were then reannealed at 1000 °C for 30 min, while the CoFeNiCr and CoFeNiMnCr were at 1000 °C for 1 h and cooled to 800 °C, and afterwards all alloys rapidly cooled in water. The ingots were then made into suitable electrodes with dimensions of 4×4×0.25 mm^3. The phase and chemical structures of the prepared electrodes were elucidated with scanning electron microscopy (SEM, Verios G4 HP), energy-dispersive X-ray spectroscopy (EDXS, Ultim Max SDD 65 mm^2) and X-ray diffraction (XRD, Malvern Panalytical Empyrean). The electrodes were then tested for an electrochemical HER using a PalmSens4 potentiostat (PalmSense BV) in a custom-designed, three-electrode cell (Fig. S2) with an in-house-developed graphite counter electrode and a reversible hydrogen electrode (RHE) as the reference electrode. The experiments were conducted in 1 M KOH and 0.5 M H_2SO_4 at approx. 20 °C. A detailed description of the material synthesis, preparation and characterization is presented in the Supplementary Information.

3. Results and discussion

3.1. Physical and chemical properties of the pristine MEAs and HEA

Configurational entropy (ΔS_{conf}) plays a vital role in classifying a multi-component alloy as either high (>1.5 R), medium (1–1.5 R), or low entropy (<1 R) [10,11]. The SEM-EDXS data from Table 1. were used to estimate the ΔS_{conf} values for the synthesized multi-component alloys. The calculated ΔS_{conf} for the CoFeNi, CoFeNiMn, CoFeNiCr, and CoFeNiMnCr were 1.1 R, 1.38 R, 1.39 R, and 1.61 R, respectively. Therefore, CoFeNi, CoFeNiMn, and CoFeNiCr can be categorized as MEAs and CoFeNiMnCr as HEA.

The microstructural analysis (Fig. 1) showed that all the MEAs solidified into large grains of up to a few mm, whereas the HEA had smaller grains of up to a few hundred μm. The CoFeNi, CoFeNiMn, and CoFeNiMnCr consisted of one primary matrix phase. The corresponding EDXS map analysis (insets of Fig. 1) of the elements comprising the matrix phase of the mentioned alloys confirmed the uniform distribution of the elements between and within the different grains on a larger scale. The HEA also had secondary phase particles in the shape of rods and blocks within the grains and at the grain boundaries. The SEM-EDXS map (insets of Fig. 1) of some particles showed enrichment in Cr and C, and depletion in Co, Fe, and Ni, while Mn was homogeneously distributed throughout the alloy. Other secondary particles were rich in Mn and O relative to other elements. The CoFeNiCr shows a more diverse microstructure of two matrix phases and a randomly distributed secondary phase, rich in Cr and C on both matrixes. These secondary phases were later on evaluated with the XRD analysis and thus assigned to $M_{23}C_6$-type carbides and Mn_2O_3 oxides. Secondary phases are often reported for MEAs and HEAs due to impurities present in the raw materials as well as contamination during the synthesis [12]. A comprehensive explanation of the structure and the formation of secondary phases in these alloys is available in our previous publication [13]. In summary, Mn oxide particles are very likely to form in multi-component alloys containing Mn, because Mn ions have a high affinity for oxygen, resulting in a prioritized reaction with oxygen ions to form oxides [14]. Furthermore, the metal ions (M) incorporated into the $M_{23}C_6$-type carbide are primarily Cr (due to its higher chemical affinity for carbon compared to the other elements), to a lesser extent Mn, and probably also other metals present in the alloy (according to theoretical studies) [15,16]. Quantitative results of the point SEM-EDXS analysis for matrix phases in all four investigated alloys are given in Table 1 and illustrated by a diagram in Fig. S3. The measured concentrations of the constituting elements (at%) in the matrix phases in CoFeNi, CoFeNiMn, and CoFeNiMnCr are in excellent agreement with the nominal compositions of the MEAs and HEA, confirming equiatomic, solid-solution alloy systems [17]. In CoFeNiCr the first matrix phase also contains equal atomic portions of all four elements, whereas the second matrix phase is noticeably richer in Cr, by about 12 at% relative to the other elements, which implies the coexistence and stability of the equi- ($Co_{25}Fe_{25}Ni_{25}Cr_{25}$) and non-equiatomic ($Co_{22}Fe_{22}Ni_{22}Cr_{34}$) phases within the synthesized CoFeNiCr alloy system.

Fig. 2 and Table S1 present the results of the XRD analysis for all the MEAs and HEA. The XRD patterns reveal that the CoFeNi, CoFeNiMn, and CoFeNiMnCr alloys exhibit a single face-centered cubic (FCC1) solid-solution structure with resolved (111), (200), (220), and (311) lattice planes. The XRD pattern of CoFeNiMnCr also shows a set of low-intensity reflections attributed to secondary phases of the cubic $M_{23}C_6$-type carbide and Mn_2O_3 oxide, as indicated by the SEM analysis. The CoFeNiCr is composed of two face-centered-cubic phases (FCC1 and FCC2) and $M_{23}C_6$-type carbides, identified by several weak reflections belonging to these impurity phases. The CoFeNi and CoFeNiCr have lower main phase reflection intensities in their XRD patterns compared to the CoFeNiMn and CoFeNiMnCr, which is attributed to the presence of larger grains, as confirmed by the SEM analysis, resulting in a smaller number of diffracting grains within the sample available for the XRD. The lattice constants of the FCC1 solid-solution phase for the CoFeNi, CoFeNiMn, and CoFeNiMnCr are 3.58 (1) Å, 3.61 (1) Å, and 3.60 (1) Å, respectively. For CoFeNiCr, the lattice parameters of the FCC1 and FCC2 are 3.53 (1) Å and 3.56 (1) Å, respectively. Although the four alloys have the same FCC1 solid-solution matrix, the lattice constants differ depending on the compositional change. In particular, the addition of Mn induces a shift of the FCC1 diffraction peaks to lower angles, leading to an expansion of the lattice constant due to the relatively larger atomic size of the Mn compared to the other elements. On the other hand, the incorporation of Cr with a small atomic radius shrinks the lattice of the FCC1 solid-solution phase [18,19]. For CoFeNiCr containing both FCC1 and FCC2 matrix phases, where FCC2 has a higher Cr content than the FCC1, the lattice constant tends to increase with an increased Cr content [20]. The lattice constants of our four alloys are comparable to the previous theoretical and experimental values reported by other researchers [9,21–23].

Table 1
Chemical composition of solid-solution matrix phases (FCC1 and FCC2) in the MEAs and HEA using SEM-EDXS point analysis.

	Composition (at%)				
	CoFeNi	**CoFeNiMn**	**CoFeNiCr**		**CoFeNiMnCr**
	FCC1	*FCC1*	*FCC1*	*FCC2*	*FCC1*
Co	30.9 ± 0.1	24.6 ± 0.5	25.7 ± 0.1	22.0 ± 0.1	20.4 ± 0.6
Fe	32.6 ± 0.1	24.4 ± 0.4	25.1 ± 0.2	22.3 ± 0.2	20.3 ± 0.1
Ni	33.5 ± 0.1	24.6 ± 0.1	25.1 ± 0.1	22.1 ± 0.1	20.0 ± 0.1
Mn	/	26.4 ± 0.1	/	/	19.0 ± 0.2
Cr	/	/	24.1 ± 0.3	33.6 ± 0.3	20.3 ± 0.5

3.2. Electrochemical properties of MEAs and HEA electrocatalysts for HERs

The electrocatalytic capabilities of the MEAs and HEA for HERs were

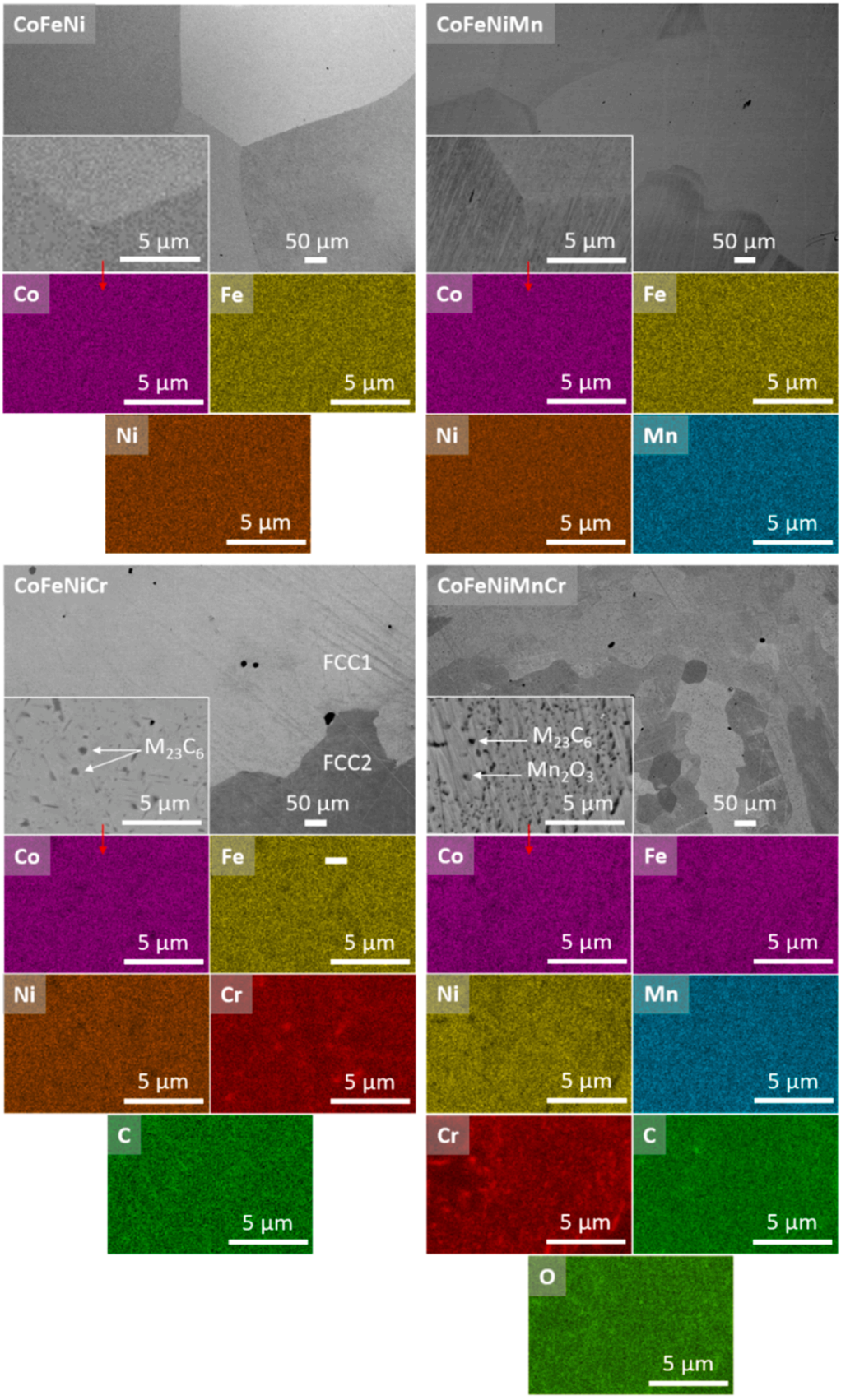

Fig. 1. SEM-BSE images and corresponding EDXS elemental maps of MEAs and HEA.

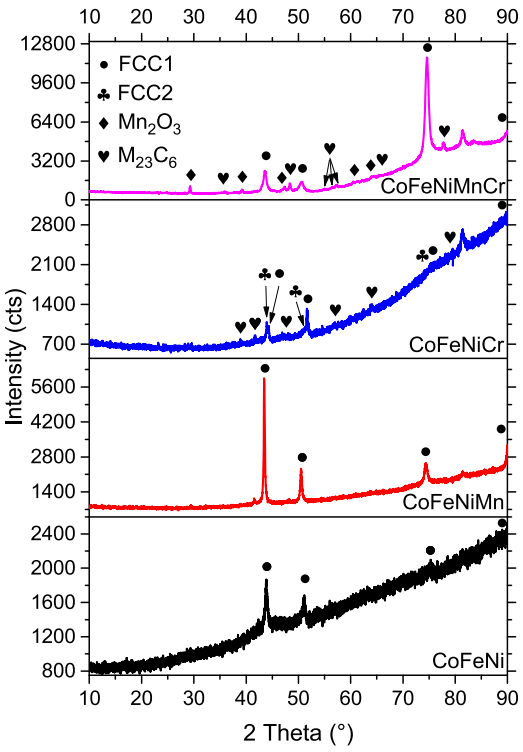

Fig. 2. XRD pattern of MEAs and HEA.

investigated with linear sweep voltammetry (LSV), electrochemical impedance spectroscopy (EIS), cyclic voltammetry (CV) and chronoamperometry (CA). All the HER kinetic parameters of the electrocatalysts in 1 M KOH and 0.5 M H_2SO_4 are presented in Table 2 and Fig. 3. Understanding the activity of the electrocatalysts for HER can be supported by the well-known Sabatier principle and a volcano plot [24]. The most active electrocatalysts should bind hydrogen atoms neither too strongly nor too weakly. Under these optimal conditions, the Gibbs free energy of hydrogen absorption (ΔG) should be zero, and the electrocatalyst should be located at the summit of the Sabatier volcano plot. The elements Co, Fe, and Ni have nearly the same negative ΔG and exhibit a relatively high hydrogen-binding ability (HBA). Cr has an even more negative ΔG than Co, Fe, and Ni, whereas Mn has a positive ΔG and thus a poor ability to bind hydrogen. Considering these, the HER kinetic parameters are evidently influenced by the composition and proportion of elements with different adsorption and desorption of hydrogen in the MEAs and HEA.

Table 2
Electrochemical parameters of MEAs and HEA (η_{10}: overpotential at 10 mA/cm^2, R_s: electrolyte resistance, R_{ct}: charge-transfer resistance).

	CoFeNi	CoFeNiMn	CoFeNiCr	CoFeNiMnCr	Pt
	1 M KOH				
η_{10} (mV vs. RHE)	326	335	338	345	281
Tafel slope (mV/dec)	192	194	167	173	217
R_s (Ω)	40.0				
R_{ct} (Ω)	38.2	41.1	42.0	47.5	32.9
C_{dl} (μF/cm^2)	17.90	12.60	10.90	5.52	24.30
ECSA	0.45	0.32	0.27	0.14	0.61
	0.5 M H_2SO_4				
η_{10} (mV vs. RHE)	299	271	486	403	128
Tafel slope (mV/dec)	204	207	130	140	166
R_s (Ω)	30.0				
R_{ct} (Ω)	15.1	14.4	85.0	63.0	12.2
C_{dl} (μF/cm^2)	55.80	62.40	1.95	4.07	76.95
ECSA	1.59	1.78	0.06	0.12	2.20

Synthesized electrocatalysts exhibited related overpotentials at 10 mA/cm^2 (η_{10}) in 1 M KOH. However, there is a noticeable trend in the overpotential to be at its lower for CoFeNi (326 mV), similar for CoFeNiMn (335 mV) and CoFeNiCr (338 mV), and the highest for CoFeNiMnCr (345 mV). The electrochemical impedance behavior of all the MEAs and HEA could be elucidated with a simplified Randle equivalent circuit consisting of the electrolyte resistance (R_s), the charge-transfer resistance over the electrolyte-electrode interface (R_{ct}), and the constant-phase element (CPE). The corresponding R_{ct} followed the same trend as η_{10}, i.e., CoFeNi (38.23 Ω) < CoFeNiMn (41.11 Ω) ≤ CoFeNiCr (42.00 Ω) < CoFeNiMnCr (47.49 Ω). On the contrary, double-layer capacitance (C_{dl}) and thus related electrochemical surface area (ECSA) are decreasing with increasing R_{ct} of the alloys. The ECSA for CoFeNi, CoFeNiMn, CoFeNiCr and CoFeNiMnCr are 0.45, 0.32, 0.27, 0.14, respectively. Presented electrochemical parameters are well interrelated. Surfaces with a higher ability to store charge in the electrical double layer (C_{dl}) formed at the interface between the electrode and electrolyte show larger surface areas with more available active sites (ECSA), which facilitate a more rapid electron transfer in reducing the resistance across the interface (R_{ct}) and thus less energy (η_{10}) is required to overcome the kinetic barrier of the HER process. Overall, the lower η_{10} and R_{ct}, higher $C_{dl,}$ and larger ECSA were reached with higher contents of the elements Co, Fe, and Ni in the alloy system. According to the Sabatier principle, Co, Fe, and Ni exhibited relatively high but seemingly optimal HBAs for an improved HER in our system. The addition of other elements, however, unbalanced the system for alkaline HER. An additional reason for the favorable electrochemical properties of compositions containing Cr could be that Cr is one of the most inert transition metals with respect to HERs because it forms a thin, protective, oxide surface layer when standing in the air or in contact with water, resulting in a delay to the HER process [25]. In contrast, the Tafel slope was lower for CoFeNiCr (167 mV/dec) and CoFeNiMnCr (173 mV/dec), while it was higher for CoFeNi (192 mV/dec) and CoFeNiMn (194 mV/dec). A lower Tafel slope indicates faster reaction kinetics. Some experimental alkaline HER studies conducted on transitional ternary and binary metals also detected a lowering of the Tafel slopes when adding Cr with higher HBA [2,26]. Namely, the lower Tafel slope of the CoFeNiCr and CofeNiMnCr could be attributed to a pronounced synergetic effect between multiple primary and secondary phases. This synergy can be explained by the well-established spillover phenomenon involving the surface dynamics of adsorbed hydrogen at the electrode surface [27]. In CoFeNiCr, based on the Sabatier principle, the Cr-rich FCC2 phase has a stronger affinity for hydrogen and is thus more prone to hydrogen adsorption or the dissociation of water (Volmer reaction), while the equi-atomic FCC1 phase with less Cr than the FCC2 phase and especially secondary carbides with a larger lattice constant [25] are more susceptible to hydrogen desorption (Heyrovski reaction). Thus, the H adatom is created on the FCC2 phase and rapidly migrates towards and reacts on the FCC1 and carbide phases to be released as molecular hydrogen. The spillover process has a positive effect on the delicate electron distribution to boost the dynamics of the reactions when starting and thus promoting the HER mechanism [28]. A similar situation applies to the CoFeNiMnCr, albeit to a lesser extent due to the presence of only one primary and carbide phases.

The electrocatalytic performance of the MEAs and HEA with respect to the HERs in 0.5 M H_2SO_4 differed from that in 1 M KOH. In terms of η_{10}, the order of the electrocatalytic activity was as follows: CoFeNiMn (271 mV) > CoFeNi (299 mV) > CoFeNiMnCr (403 mV) > CoFeNiCr (486 mV). The differences in η_{10} for these compositions were also larger. R_{ct} was very low for CoFeNiMn (14.44 Ω) and CoFeNi (15.11 Ω), whereas it was much higher for CoFeNiMnCr (63.01 Ω) and CoFeNiCr (85.00 Ω). Furthermore, the ECSA values decreased as opposed to η_{10} and R_{ct} (CoFeNiMn: 1.78, CoFeNi: 1.59, CoFeNiMnCr: 0.12, CoFeNiCr: 0.06). The trend between the η_{10}, R_{ct}, C_{dl} and ECSA values coincided

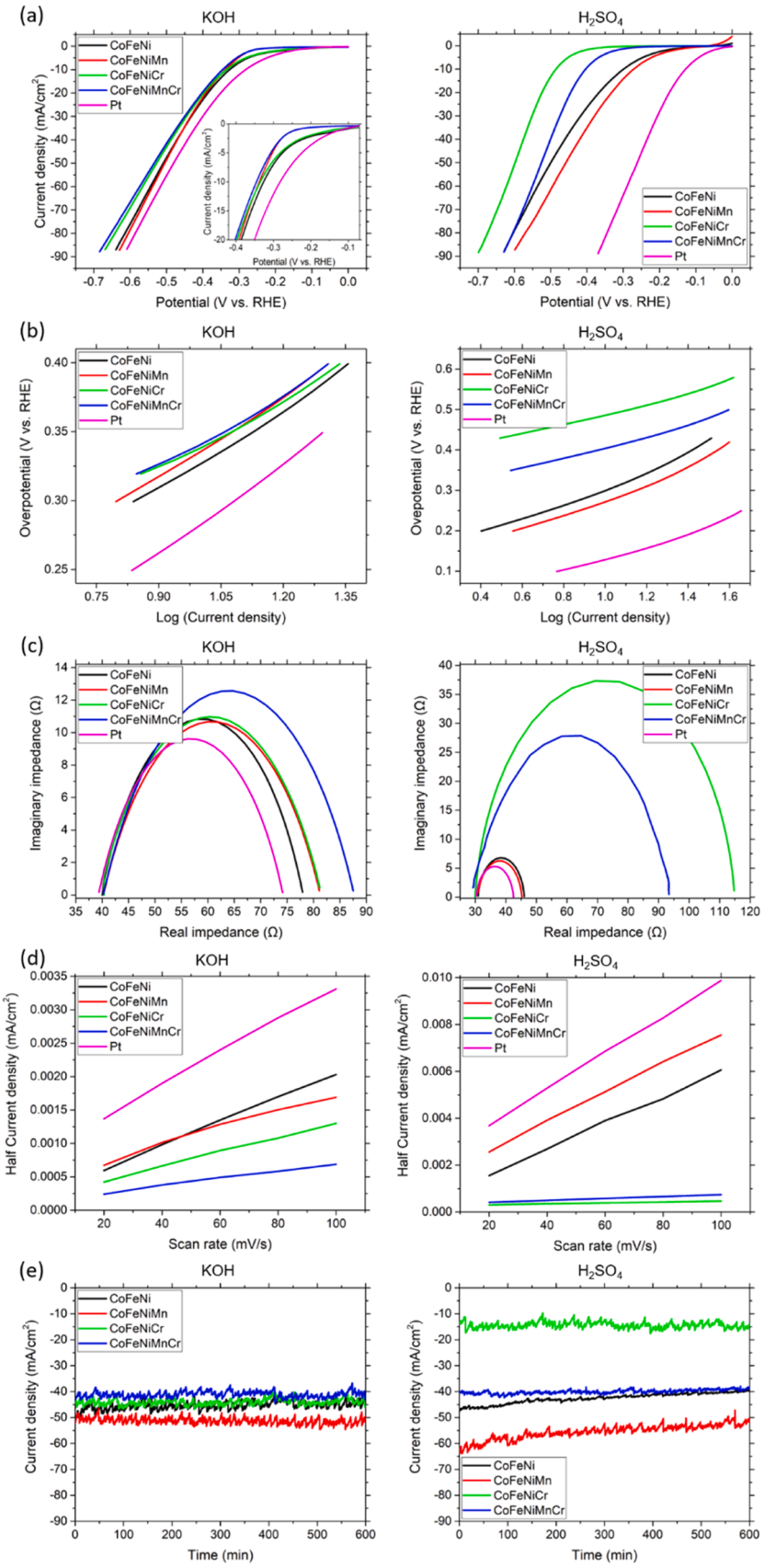

Fig. 3. LSV (a), Tafel (b), Nyquist (c), and CA (d) graphs for all the MEAs and the HEA in 1 M KOH and 0.5 M H_2SO_4.

with the ones observed in 1 M KOH. Adding elements with lower inertness and HBA resulted in a decreasing η_{10}/R_{ct} and increasing C_{dl}/ECSA for acidic HER, similar to the alkaline HER. Furthermore, CoFeNi showed improved electrochemical properties in alkaline media compared to other alloys due to the aforementioned reason, whereas on the contrary, the superior behavior of CoFeNiMn in acidic media can be attributed to the sluggish nucleation of the surface and hence the formation also of a larger physical surface area during pre-activation step because of the presence of less stable Mn in an acidic environment, leading to a larger number of active sites to boost the HER process [29]. The Tafel slopes for CoFeNi, CoFeNiMn, CoFeNiCr, and CoFeNiMnCr in 0.5 M H_2SO_4 were 204 mV/dec, 207 mV/dec, 130 mV/dec, and 140 mV/dec, respectively. They followed the same trend as those in 1 M KOH; specifically, MEA and HEA with higher HBA elements decreased the Tafel slope. Moreover, the CoFeNi and CoFeNiMn with lower η_{10} exhibited a higher Tafel slope and vice versa for the CoFeNiCr and CoFeNiMnCr. As in 1 M KOH, also in 0.5 M H_2SO_4, the lower Tafel slope exhibited CoFeNiCr and CoFeNiMnCr, attributed to their diverse microstructure.

Overall, electrochemical parameters indicated that the HER on all the MEAs and the HEA in both 1 M KOH and 0.5 M H_2SO_4 proceeded through the Volmer–Heyrovsky mechanism, with the Volmer reaction (electrochemical adsorption or water dissociation) being the rate-determining step. Additionally, CoFeNi and CoFeNiMn had a lower η_{10} but a higher Tafel slope compared to CoFeNiCr and CoFeNiMnCr in both media, which suggests a trade-off between kinetic activity (energy input) and efficiency (conversion of the energy into reaction) in catalyzing the HER. Nevertheless, the prepared electrocatalysts showed similar or even better catalytic activity with respect to the HER than commercial Pt foil (Table 2 and Fig. 3) in our HER system. The HER performance was also compared with the recently reported CoFeNiXY (XY: Mn and/or Cr) catalysts, which are listed in Table S2.

The stability of all the MEAs and the HEA in both media was also tested via CA for 10 h. The results are shown in Fig. 2d. All the MEAs and HEA in 1 M KOH, as well as CoFeNiCr and CoFeNiMnCr in 0.5 M H_2SO_4, maintained a stable current density. In contrast, CoFeNi and CoFeNiMn retained only 90 % and 75 % of the current density in 0.5 M H_2SO_4, respectively. The SEM analysis (Fig. S4) after the stability test in 1 M KOH showed no changes in the surface structure of all the MEAs and HEA. Also, no metal ions were detected in the electrolyte when using an ICP-OES analysis (Table S3). These confirmed the good long-term stability of all the MEAs and the HEA for alkaline HER. However, some surfaces of the MEAs and HEA after the stability test in 0.5 M H_2SO_4 (Fig. S5) were nevertheless noticeably changed. Over the entire surfaces of the CoFeNi and CoFeNiMn there were etched imprints of H_2 bubbles, while the CoFeNiCr and CoFeNiMnCr surfaces were only partially etched in areas with a higher density of secondary phases. The ICP-OES analysis (Table S3) showed the highest presence of metal ions in the acidic electrolyte for CoFeNiMn, half as much for CoFeNi, and moderate amount for CoFeNiMnCr and CoFeNiCr. Furthermore, the concentration of dissolved metal ions was equimolar for all the MEAs and the HEA, which probably originated from the electrochemical process itself to preserve the original atomic ratio of the elements in the electrocatalysts [30]. Based on these results, the compositions with Cr, especially CoFeNiCr, showed the best stability owing to the complex microstructure and good corrosion resistance of Cr in acidic media, as described previously [31].

Nevertheless, the compositions without Cr showed an improved catalytic activity, while the compositions with Cr, and thus a more diverse microstructure, showed a higher catalytic efficiency and stability in both media. Choosing between a catalyst with better activity or better stability depends on a thorough evaluation of the specific requirements and constraints of the application. However, utilizing multi-component alloys as HER electrocatalysts could be an opportunity to choose between highlighted activity or stability, or even to find a proper balance between activity and stability by varying the elemental concentrations and compositions.

4. Conclusions

CoFeNi, CoFeNiMn, CoFeNiCr, and CoFeNiMnCr with crystalline structures were successfully prepared with a direct and simple inert-gas melting process. The prepared MEA and HEA electrocatalysts exhibited promising electrocatalytic activity, compared to Pt foil, for both alkaline and acidic HERs. The overall catalytic activity was described as a function of the interaction between the catalysts and reactive hydrogen intermediates. This relationship exhibited a trend in overpotential for alkaline and acidic media as follows: CoFeNi < CoFeNiMn <= CoFeNiCr < CoFeNiMnCr and CoFeNiMn < CoFeNi < CoFeNiMnCr < CoFeNiCr, respectively. The overpotential in alkaline media is mainly triggered by the proportion of Co, Fe, and Ni in the alloy since only this elemental combination demonstrated the optimal HBA for HER. In acidic media, all the elements contribute to the outcoming overpotential, which is improved when elements with higher HBA are selected. The Tafel slope followed the same trend in both media as CoFeNiCr < CoFeNiMnCr < CoFeNi < CoFeNiMn. A lower Tafel slope is observed for alloys containing multiple phases in synergy, known as the spillover process. Furthermore, all the MEA and HEA electrocatalysts had excellent stability in alkaline media, whereas the compositions with Cr showed favorable stability in acidic media due to the complex microstructures and elemental resistance. These findings highlight the uniqueness of entropy alloys for designing and utilizing good electrocatalysts with adjustable properties (activity and/or stability) for different HER systems.

CRediT authorship contribution statement

Maja Ponikvar-Svet: Methodology, Formal analysis. **Lara Einfalt:** Visualization. **Miran Čeh:** Writing – review & editing, Visualization, Supervision, Resources, Project administration, Methodology, Funding acquisition. **Barbara Ljubec Božiček:** Writing – original draft, Methodology, Formal analysis, Data curation, Conceptualization. **Belisa Alcantara Marinho:** Writing – review & editing, Supervision, Project administration, Methodology, Funding acquisition, Conceptualization. **Iztok Naglič:** Validation, Methodology, Investigation, Formal analysis. **Boštjan Markoli:** Writing – review & editing, Visualization, Resources. **Bor Arah:** Writing – review & editing, Methodology, Formal analysis. **Monika Kušter:** Methodology, Formal analysis.

Declaration of Competing Interest

The authors declare that they have no known competing financial interests or personal relationships that could have appeared to influence the work reported in this paper.

Acknowledgments

The authors gratefully acknowledge the Slovenian Research Agency for financial support in projects P2-0084 and PR-11484. This work has also received funding from the European Union's Horizon research and innovation programme under the HORIZON-WIDERA-2022-TALENTS-02 grant agreement No. 101090289.

Appendix A. Supporting information

Supplementary data associated with this article can be found in the online version at doi:10.1016/j.mtcomm.2024.110876.

Data availability

Data will be made available on request.

References

[1] A. Pareek, R. Dom, J. Gupta, J. Chandran, V. Adepu, P.H. Borse, Insights into renewable hydrogen energy: Recent advances and prospects, Mater. Sci. Energy Technol. 3 (2020) 319–327, https://doi.org/10.1016/j.mset.2019.12.002.

[2] Y. Du, B. Li, G. Xu, L. Wang, Recent advances in interface engineering strategy for highly-efficient electrocatalytic water splitting, InfoMat 5 (2022) 12377, https://doi.org/10.1002/inf2.12377.

[3] Z. Chen, W. Wei, B.-J. Ni, Cost-effective catalysts for renewable hydrogen production via electrochemical water splitting: Recent advances, Curr. Opin. Green. Sustain. Chem. 27 (2021) 100398, https://doi.org/10.1016/j.cogsc.2020.100398.

[4] Q. Yu, Z. Zhang, H. Liu, X. Kang, S. Ge, S. Li, L. Gan, B. Liu, Why do platinum catalysts show diverse electrocatalytic performance? Fundam. Res. 3 (2023) 804–808, https://doi.org/10.1016/j.fmre.2022.03.017.

[5] X. Yang, R. Guo, R. Cai, Y. Ouyang, P. Yang, J. Xiao, Engineering high-entropy materials for electrocatalytic water splitting, Int. J. Hydrog. Energy 47 (2022) 13561–13578, https://doi.org/10.1016/j.ijhydene.2022.02.123.

[6] D.B. Miracle, O.N. Senkov, A critical review of high entropy alloys and related concepts, Acta Mater. 122 (2017) 448–511, https://doi.org/10.1016/j.actamat.2016.08.081.

[7] S.A. Ali, S.M. Alshehri, T. Ahmad, Rational integration of MoSe2 and BN with TiO2 to design nanoengineered ternary heterojunctions for sustainable hydrogen energy: Experimental evidences and theoretical anticipations, Int. J. Hydrog. Energy 82 (2024) 1182–1195, https://doi.org/10.1016/j.ijhydene.2024.08.043.

[8] J. Hao, Z. Zhuang, K. Cao, G. Gao, C. Wang, F. Lai, S. Lu, P. Ma, W. Dong, T. Liu, M. Du, H. Zhu, Unraveling the electronegativity-dominated intermediate adsorption on high-entropy alloy electrocatalysts, Nat. Commun. 13 (2022) 2662, https://doi.org/10.1038/s41467-022-30379-4.

[9] F. McKay, Y. Fang, O. Kizilkaya, P. Singh, D.D. Johnson, A. Roy, D.P. Young, P. T. Sprunger, J.C. Flake, W.A. Shelton, Y. Xu, CoCrFeNi High-Entropy Alloy as an Enhanced Hydrogen Evolution Catalyst in an Acidic Solution, J. Phys. Chem. C. (2021), https://doi.org/10.1021/acs.jpcc.1c03646.

[10] J.-W. Yeh, Alloy Design Strategies and Future Trends in High-Entropy Alloys, JOM 65 (2013) 1759–1771, https://doi.org/10.1007/s11837-013-0761-6.

[11] O.F. Dippo, K.S. Vecchio, A universal configurational entropy metric for high-entropy materials, Scr. Mater. 201 (2021) 113974, https://doi.org/10.1016/j.scriptamat.2021.113974.

[12] E.J. Pickering, R. Muñoz-Moreno, H.J. Stone, N.G. Jones, Precipitation in the equiatomic high-entropy alloy CrMnFeCoNi, Scr. Mater. 113 (2016) 106–109, https://doi.org/10.1016/j.scriptamat.2015.10.025.

[13] B.L. Božičček, J. Hreščak, M. Kušter, J. Kovač, I. Naglič, B. Markoli, B.Š. Batič, M. Šala, S. Drev, Ž. Marinko, M. Čeh, B.A. Marinho, Unveiling the potential of (CoFeNiMnCr)3O4 high-entropy oxide synthesized from CoFeNiMnCr high-entropy alloy for efficient oxygen-evolution reaction, J. Mater. Sci. 59 (2024) 9189–9207, https://doi.org/10.1007/s10853-024-09710-5.

[14] D. Jiang, Z. Li, J. Xu, Q. Ren, S.-O. Agbedor, Q. Lei, High-temperature oxidation behaviors of an equiatomic CrMnFeCoNi high entropy alloy, Mater. Today Commun. 32 (2022) 104185, https://doi.org/10.1016/j.mtcomm.2022.104185.

[15] A. Heidarpour, M. Faraji, A. Haghighi, Production and characterization of carbide-derived-nanocarbon structures obtained by HF electrochemical etching of Ti3AlC2, Ceram. Int. 48 (2022) 11466–11474, https://doi.org/10.1016/j.ceramint.2022.01.003.

[16] R. Besson, Understanding phase equilibria in high-entropy alloys: II. Atomic-scale study of incorporation of metallic elements in Cr carbides – Application to equilibrium with AlCrFeMnMo, J. Alloys Compd. 874 (2021) 159959, https://doi.org/10.1016/j.jallcom.2021.159959.

[17] F. Da Costa Garcia Filho, R.O. Ritchie, M.A. Meyers, S. Neves Monteiro, Cantor-derived medium-entropy alloys: bridging the gap between traditional metallic and high-entropy alloys, J. Mater. Res. Technol. 17 (2022) 1868–1895, https://doi.org/10.1016/j.jmrt.2022.01.118.

[18] C.-C. Yen, G.-R. Huang, Y.-C. Tan, H.-W. Yeh, D.-J. Luo, K.-T. Hsieh, E.-W. Huang, J.-W. Yeh, S.-J. Lin, C.-C. Wang, C.-L. Kuo, S.-Y. Chang, Y.-C. Lo, Lattice distortion effect on elastic anisotropy of high entropy alloys, J. Alloy. Compd. 818 (2020) 152876, https://doi.org/10.1016/j.jallcom.2019.152876.

[19] W. He, C. Zeng, W. Yang, W. Chen, Y. Ai, Impact of different Cr contents on microstructural evolution and mechanical behaviour of CoCrxCuFeMnNiV high-entropy alloys, J. Mater. Res. Technol. 21 (2022) 4577–4590, https://doi.org/10.1016/j.jmrt.2022.11.072.

[20] W. Fang, H. Yu, R. Chang, X. Zhang, P. Ji, B. Liu, J. Li, X. Qu, Y. Liu, F. Yin, Microstructure and mechanical properties of Cr-rich Co-Cr-Fe-Ni high entropy alloys designed by valence electron concentration, Mater. Chem. Phys. 238 (2019) 121897, https://doi.org/10.1016/j.matchemphys.2019.121897.

[21] N.K. Adomako, J.H. Kim, Y.T. Hyun, High-temperature oxidation behaviour of low-entropy alloy to medium- and high-entropy alloys, J. Therm. Anal. Calorim. 133 (2018) 13–26, https://doi.org/10.1007/s10973-018-6963-y.

[22] S. Zhang, G. Wang, Predicting mechanical properties of high entropy alloys with face centered cubic structure from first principles calculations, Mater. Today Commun. 32 (2022) 104059, https://doi.org/10.1016/j.mtcomm.2022.104059.

[23] O. Zhang, S. Zhang, J. Hou, K. Li, M. Zhu, Z. Jie, L. Yao, Y. Liu, Z. Jian, Influence of interstitial carbon content on the microstructure, mechanical and electrochemical corrosion properties of CoFeNiMn multi-principal component alloys, J. Mater. Res. Technol. 27 (2023) 5291–5304, https://doi.org/10.1016/j.jmrt.2023.11.006.

[24] J. Zhu, L. Hu, P. Zhao, L.Y.S. Lee, K.-Y. Wong, Recent Advances in Electrocatalytic Hydrogen Evolution Using Nanoparticles, Chem. Rev. 120 (2020) 851–918, https://doi.org/10.1021/acs.chemrev.9b00248.

[25] W.-F. Chen, J.T. Muckerman, E. Fujita, Recent developments in transition metal carbides and nitrides as hydrogen evolution electrocatalysts, Chem. Commun. 49 (2013) 8896–8909, https://doi.org/10.1039/C3CC44076A.

[26] Y. Du, B. Li, G. Xu, L. Wang, Recent advances in interface engineering strategy for highly-efficient electrocatalytic water splitting, InfoMat 5 (2023) e12377, https://doi.org/10.1002/inf2.12377.

[27] F. Rosalbino, S. Delsante, G. Borzone, E. Angelini, Correlation of microstructure and catalytic activity of crystalline Ni–Co–Y alloy electrode for the hydrogen evolution reaction in alkaline solution, J. Alloy. Compd. 429 (2007) 270–275, https://doi.org/10.1016/j.jallcom.2006.03.090.

[28] Q. Zhang, M. Du, Y. Xiao, L. Wu, J. Qian, C. Zhang, Y. He, Effects of molybdenum content and heat treatment on hydrogen evolution reaction properties and microstructure of FeCoCrNiMox high entropy alloys, Intermetallics 168 (2024) 108230, https://doi.org/10.1016/j.intermet.2024.108230.

[29] H. Wang, Y. Yang, J. Liu, H. Wu, K. Wu, C. Lyu, J. Wu, W.-M. Lau, Q. Wu, J. Zheng, The role of manganese-based catalyst in electrocatalytic water splitting: Recent research and progress, Mater. Today Phys. 36 (2023) 101169, https://doi.org/10.1016/j.mtphys.2023.101169.

[30] H.H. Farrag, A.A. Abbas, S.Y. Sayed, H.H. Alalawy, B.E. El-Anadouli, A. M. Mohammad, N.K. Allam, From Rusting to Solar Power Plants: A Successful Nano-Pattering of Stainless Steel 316L for Visible Light-Induced Photoelectrocatalytic Water Splitting, ACS Sustain. Chem. Eng. 6 (2018) 17352–17358, https://doi.org/10.1021/acssuschemeng.8b04899.

[31] A. Wetzel, M. von der Au, P.M. Dietrich, J. Radnik, O. Ozcan, J. Witt, The comparison of the corrosion behavior of the CrCoNi medium entropy alloy and CrMnFeCoNi high entropy alloy, Appl. Surf. Sci. 601 (2022) 154171, https://doi.org/10.1016/j.apsusc.2022.154171.